A STAP anti-interference technology with zero phase bias in wireless IoT systems based on high-precision positioning

Fang Hao[1,2,3], Xin Li[1], Wei Wang[1]* and Jun Zhao[2,3]

[1]College of Intelligent Systems Science and Engineering, Harbin Engineering University, Harbin, China,
[2]The 54th Research Institute of China Electronics Technology Group Corporation, Shijiazhuang, China,
[3]State Key Laboratory of Satellite Navigation System and Equipment Technology, Shijiazhuang, China

Fog computing has been applied to the data processing for the Internet of Things (IoT) based on distributed high-precision Global Navigation Satellite Systems (GNSS). However, the space-time adaptive processing (STAP) interference suppression technology in the system will cause fog computing data deviation that includes carrier phase bias and pseudocode offset. An unbiased STAP technique is proposed to eliminate these deviations. First, it is analyzed that the carrier phase bias and pseudocode offset are caused by the non-linear phase response of the STAP equivalent filter. Then, a coefficient-constrained method based on practical engineering processing is proposed, which can eliminate these deviations by restricting the tap coefficients to be symmetrically equal around the center-tap. Moreover, by analyzing the coherent integral function of the pseudocode after filtering, the tap structure of STAP is modified to eliminate the group offset of the pseudocode without increasing the computational complexity and hardware resources. Finally, the unbiased performance and anti-interference performance of the system are verified by numerical and real data simulations.

KEYWORDS

Internet of Things, STAP, high-precision, anti-interference, fog computing, GNSS

1 Introduction

With the development of the Internet of Things (IoT) based on 5G + new infrastructure and Beidou satellite services, fog computing has been applied to the data processing for the IoT based on distributed high-precision positioning systems, which ensures lower communication delay and higher positioning efficiency [1–3]. However, since the navigation signal is weak, the data broadcast/reception of each fog computing node is easily interfered [4, 5]. In [6, 7], space-time adaptive processing (STAP) based on the array antenna is used to solve this problem, which places a FIR filter after each array element. This filter can process more interferences in the frequency domain without increasing the array size.

Currently, many STAP techniques have been proposed. These techniques can cancel the strong power interference, but will cause distortion of the desired signal [8–11]. Simulations and experiments show that STAP may introduce errors of more than 10 m or even a hundred meters into GNSS measurement data processed by fog calculation [12, 13]. Fante el [14]. Proposed a filter with conjugate inverse of STAP filter to eliminate phase deviation. This strategy widens the cross-coherent peak of the pseudocode and consumes more hardware

resources. Wu et al. [15] proposed a homomorphic filter that performs frequency domain processing on the original filter to compensate for errors. Frequency domain processing is complex and takes up more memory cells. O'Brien AJ el [16, 17]. Proposed an optimal adaptive filtering method for STAP, which can maximize the carrier to noise ratio without generating measurement bias. This method requires constructing a constraint matrix based on the incident angle and the signal power spectral density, which has high computational complexity and cannot be applied to engineering implementation. References [18–20] all constrain the filter coefficients to eliminate the carrier phase bias and pseudocode offset on the premise of ensuring the linear phase response of the FIR filter. However, the method of reference [18] cannot correct the carrier phase bias. Reference [19] does not give a closed-form solution of its method. The strategy proposed by Xu et al. [20] is a solution of [19], but requires complex operations, such as block matrix processing and multi beam forming. All these methods, due to the STAP filter structure, still have a constant pseudocode offset due to the STAP filter structure which has to be compensated in the receiver tracking loop [21]. To eliminate this constant offset, Marathe et al. [22] proposed a single-tap output strategy, which only outputs the data of the reference tap. But the system response of this method is non-linear, the carrier bias is generated.

Motivated by mentioned above, this paper proposes an unbiased STAP strategy. First, the measurement bias caused by the non-linear response of the STAP filter in the IoT system is analyzed based on distributed high-precision positioning and fog computing. Then, an anti-interference strategy that constrains the tap coefficients to be symmetrically equal about the center tap is proposed based on linear-phase FIR filter. Meanwhile, by analyzing the coherent integral function of the pseudocode, the tap structure of STAP is modified to achieve null offset of the pseudocode without increasing the computational complexity and hardware resources. Finally, the experiments are conducted and the results validate the effectiveness of the proposed schemes.

The rest of this paper is organized as follows. Section 1 discusses the array modeling and Section 3 provides the proposed unbiased anti-interference strategy. In Section 4, the algorithm performance is simulated and evaluated by various experiments and finally, Section 5 concludes this paper.

2 Related work

1) Adaptive Beamforming in IoT Scenarios

With the development of wireless network transmission technology and the introduction of intelligent IoT, the demand for anti-interference is increasing for wireless IoT application scenarios based on high-precision positioning systems such as intelligent transportation and unmanned driving. Adaptive beamforming technology (ADBF) can meet this requirement, which enhances the array receive gain while suppressing interference. Therefore, it has attracted more and more attention.

ADBF has become one of the symbols of array signal processing. Its essence is to use some optimal criterion to perform weighted filtering on the signals of each array element, which can enhance the desired signal and suppress the interference. And the weights can be

adaptively updated according to the interference environment. Common guidelines are.

* Maximum Signal-to-Noise Ratio (MSNR): Maximizes the ratio of desired signal power to noise power.
* Maximum Signal to Interference and Noise Ratio (MSINR): Maximizes the ratio of desired signal power to the sum of interference power and noise power.
* Minimum Mean Squared Error (MMSE): Minimizes the mean squared error between the array output and the desired response.
* Linear Constrained Minimum Variance (LCMV): Minimizes the variance of the array output under certain constraints.

This paper improves the Capon beamformer that utilizes the LCMV criterion. The beamformer tries to minimize the power of noise and interference while keeping the signal power in the observation direction θ constant. The optimization problem with constraints can be formulated as

$$\begin{cases} \min_{w} \{P_{out} = w^H R_x w\} \\ s.t.\ w^H a(\theta) = 1 \end{cases} \quad (1)$$

where P_{out} is the signal power, and w is the array weight. R_x and $a(\theta)$ represent the array covariance matrix and the steering vector of the desired signal, respectively. In Eq. (1), the sub-constraint guarantees the output power of the desired signal, and the main constraint achieves the purpose of suppressing the interference and noise by minimizing the output power. The classic adaptive beamforming anti-interference schemes and their main contributions are summarized in Table 1 as follows.

2) FIR filter

An intermediate frequency (IF) sampled data is processed based on the STAP in this paper. STAP is based on a finite impulse response (FIR) filter that is one of the crucial parts to digital signal processing. The FIR filter has two advantages of realizability and linear phase, so it is widely used in practice. Khan et al. present least squares (LS) approach to design linear phase FIR filter [27]. Wang et al. proposed new structures of type II, III and IV linear phase FIR systems [28]. In this paper, the linear phase FIR filter is used to improve the spatiotemporal two-dimensional beamformer in the wireless IoT system based on distributed high-precision positioning.

3 Array model of wireless Internet of Things systems

The structure of wireless IoT system based on distributed high-precision positioning and fog computing is shown in Figure 1. Assuming an ideal hardware environment, the mixed signal is received by an N-element linear array with half-wavelength equidistant, which can be written as

$$x(t) = \sum_{k=0}^{P} a_k s_k(t) + n(t) \quad (2)$$

where $x(t) = [x_1(t)\quad x_2(t)\quad \dots\quad x_N(t)]^T$. The subscript $k = 0$ represents the navigation signal, and $k = 1, 2, \dots, P$ represents the

TABLE 1 The classical ADBF based LCMV schemes.

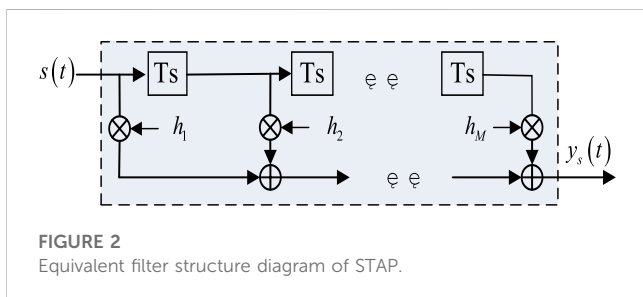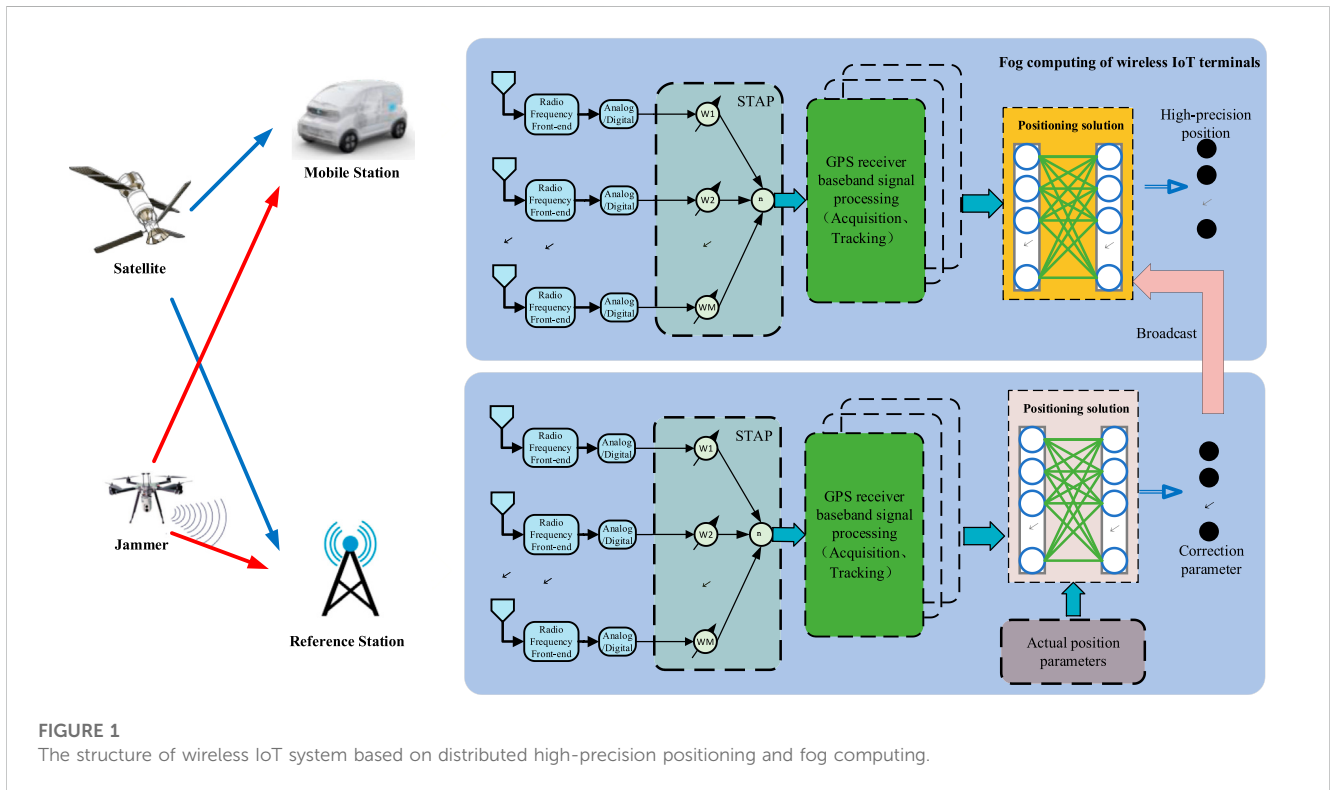| Index	Tittle	Contribution
[23]	MWF-NW Algorithm for Space-Time Antijamming	A beamforming algorithm based on multistage wiener filter is proposed
[6]	Robust Wideband Adaptive Beamforming with Null Broadening and Constant Beamwidth	Frequency Domain Beamforming Based on STAP.
[24]	A robust STAP beamforming algorithm for GNSS receivers in high dynamic environment	A STAP algorithm based on covariance matrix reconstruction is proposed in high dynamic environment
[25]	A Robust Beamformer Based on Magnitude Response Constraint and Steering Vector Correction	An ADBF without beam direction mismatch is proposed
[26]	A Robust Anti-Jamming Navigation Receiver with Antenna Array and GPS/SINS.	An ADBF based on GPS/SINS-aided is proposed

FIGURE 1
The structure of wireless IoT system based on distributed high-precision positioning and fog computing.

FIGURE 2
Equivalent filter structure diagram of STAP.

interference. a, $s(t)$ and $n(t)$ are the steering vector, the received signal and the Gaussian white noise, respectively. The expression of the navigation signal is

$$s_0(t) = A_0 p(t - \tau_0) \exp\left(j2\pi f_{IF} t + j\varphi_0\right) \quad (3)$$

where A_0, $p(t)$, τ_0, f_{IF} and φ_0 are the amplitude of the navigation signal, the corresponding pseudocode sequence, pseudocode shift, the IF and the initial carrier phase, respectively.

Assumed that each element has an M-tap FIR filter in the STAP structure, where the delay interval is T_s. The equivalent filter structure of STAP is shown in Figure 2. After space-time filtering, the output can be indicated as:

$$
\begin{aligned}
y_s(t) &= \sum_{n=1}^{N}\sum_{m=1}^{M} w_{nm}^{*} x(t - (m-1)T_s) \\
&= \sum_{m=1}^{M} w_{m}^{H} a_0 s(t - (m-1)T_s) \\
&= H(f, \theta) \cdot s(t)
\end{aligned}
\quad (4)
$$

where $w_m = [w_{1m} \quad w_{2m} \quad \ldots \quad w_{Nm}]^T$ is the weight vector on the $m-1$ th delay node. The sampling interval is described as T_s. $H(f, \theta)$ is the filter transfer function. If $H(f, \theta) = 1$, the tracking result of the satellite signal is unbiased. However, in practice, the amplitude-frequency response of the STAP transfer function is not flat and the phase-frequency response is non-linear, resulting in the estimated bias of the carrier/pseudocode phase. Decompose $H(f, \theta)$ to get the amplitude-frequency response and the phase-frequency response.

$$H(f, \theta) = |H(f, \theta)|e^{ja(f, \theta)} \tag{5}$$

where $|\cdot|$ is the modulo value. Perform Taylor expansion on the phase term of the transfer function, that is, $a = a_0 + a_1 f + a_2 f^2 + .$ quadratic terms and higher-order terms are ignored, and the correlation function of the tracking loop is expressed as

$$R_1(\tau, \theta) = cA_0 \int_{-\infty}^{\infty} \Phi(f)|H(f, \theta)|e^{j(\psi_0 + a_0)}e^{j2\pi f(\tau - \tau_0 + a_1)}df \tag{6}$$

From Eq. (6), the estimated pseudocode phase offset is $\tau_0 - a_1$, and the corresponding carrier phase is $\psi_0 + a_0$. Therefore, the spatiotemporal data processing structure causes pseudocode phase-shift and carrier offset, which will reduce the accuracy of fog computing. Furthermore, different bias will be generated for signals from different directions.

4 The proposed STAP under wireless Internet of Things conditions

According to the analysis of measurement bias introduced by the non-linear response of STAP in Section 3, an unbiased STAP strategy is proposed. First, a filter that satisfies the linear phase response is analyzed. After that, this strategy ensures the equivalent filter linear phase response by constraining the tap coefficients to be symmetrically equal about the center tap. Finally, the STAP filter structure was modified by analyzing the coherent integral function of the pseudocode filtered by STAP. The null bias is achieved so that a generic receiver can be interfaced with the STAP processor without modifying the tracking loop. Therefore, the proposed strategy can not only suppress interference to ensure unbiased reception of signals, but also does not modify the tracking loop of generic receivers.

For a filter with a linear phase response, the frequency characteristics of the system satisfy the following relationship [29].

$$\varphi(\omega) = \beta - \alpha\omega \tag{7}$$

where $\varphi(\omega)$ is the phase function with respect to the angular frequency ω. β and α are constant coefficients. The group delay of the system is $\tau_g = -d\varphi/d\omega = \alpha$. When $\beta = 0$, $\varphi(\omega) = -\alpha\omega$. This FIR is strict linear phase.

Suppose the unit impulse response of the FIR is $h(q), 0 \le q \le Q-1$, and it is necessary to satisfy $h(0) \ne 0$ and $h(Q-1) \ne 0$. The discrete-time Fourier transform (DTFT) of an FIR that satisfies strict linear phase is expressed as follows

$$\begin{aligned} H(e^{j\omega}) &= H(\omega)e^{j\varphi(\omega)} \\ &= H(\omega)e^{-j\omega\alpha} \\ &= \sum_{q=0}^{Q-1} h(q)e^{-j\omega n} \end{aligned} \tag{8}$$

where $H(\omega)$ is a positive or negative real function. Since the real and imaginary parts in Eq. (8) are each equal, the ratio of the real part to the imaginary part can be written as follows

$$\frac{sin(\alpha\omega)}{cos(\alpha\omega)} = \frac{\sum_{q=0}^{Q-1} h(q) sin(\omega q)}{\sum_{q=0}^{Q-1} h(q) cos(\omega q)} \tag{9}$$

Eq. 10 performs the crossover-multiplication operations to get

$$\sum_{q=0}^{Q-1} h(q) sin[(\alpha - q)\omega] = 0 \tag{10}$$

Eq. 10 is a necessary condition for FIR to satisfy strictly linear phase. It is easy to know that the constraint that makes Eq. 9 hold constant for any $\omega \in \mathbb{R}$ is

$$\begin{cases} \alpha = \dfrac{Q-1}{2} \\ h(q) = h(Q-1-q), \ 0 \le q \le Q-1 \end{cases} \tag{11}$$

The above equation shows that there is a linear phase characteristic with a phase delay $\alpha = (Q-1)/2$ for any Q value, and $h(q)$ must be evenly symmetric with respect to α. In practical engineering, the input of the generic receiver is a real signal whose data has only the real part. It can be expressed as

$$y_{input}(t) = real(y_s) = real\left(\sum_{m=1}^{M} h(m)s(t - (m-1)T_s)\right) \tag{12}$$

where the filter coefficients are $h(m) = w_m^H a_0$, $real(\cdot)$ represents the extraction of real part. Also, the input signal of the anti-interference module is real data in practical engineering. Therefore, it can be found from Eq. 12 that the output signal of STAP is mainly affected by the real part of the filter coefficient. To ensure that the phase-frequency response of the STAP filter is linear, the unbiased strategy based on the linear phase-response FIR filter criterion is as follows

$$w = argminwE[X(t)X^H(t)]w = argminwR_xw$$
$$s.t. \begin{cases} w_m^H a(\theta) = w_{M-m+1}^H a(\theta) \\ w_{(M+1)/2}^H a(\theta) = 1 \\ M \text{ is } odd \end{cases} \bigg| , m = 1, 2, \ldots, \frac{(M-1)}{2} \tag{13}$$

where $X(t) = [x^T(t), x^T(t - T_s), \ldots, x^T(t - (M-1)T_s)]^T$ is an $MN \times 1$-dimensional matrix. The first constraint guarantees a linear phase-frequency response, and the second allows the signal to be received without distortion. Eq. 13 can be calculated by the Lagrange multiplier algorithm.

First, the constraints in Eq. 13 are represented in matrix. Let

$$C = diag\left[\underbrace{a(\theta), \ldots, a(\theta)}_{M}\right] = [c_1, \ldots, c_M] \tag{14}$$

The constraints can be written as

$$\begin{cases} c_m^H w - c_{M-m+1}^H w = 0, m = 1, 2, \ldots, \dfrac{(M-1)}{2} \\ c_{(M+1)/2}^H w = 1 \end{cases} \tag{15}$$
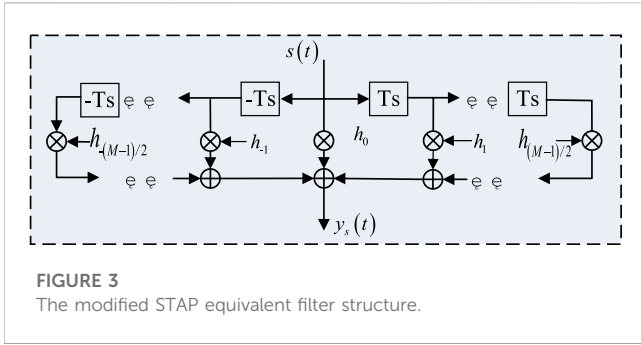
FIGURE 3
The modified STAP equivalent filter structure.

TABLE 2 Basic signal parameters.

Start and end	Signal types	DOA/deg	SNR/INR
t = 0–0.6s	B1	0	−20 dB
t = 0.6s–1.2s	B1	0	−20 dB
	WCW	−55	70 dB
t = 1.2s–1.5s	B1	0	−20 dB
	WCW	−45	80 dB
	WGN	30	70 dB

Further, let

$$l_1 = \left[c_1, \ldots, c_{(M+1)/2} \right] \tag{16}$$

$$l_2 = \left[c_M, c_{M-1} \ldots, c_{(M+3)/2}, 0 \right] \tag{17}$$

$$\bar{w} = [w_r, w_i]^T \tag{18}$$

where w_r and w_i are the real and imaginary parts of the array weight vector, respectively. Eq. 15 can be written as

$$
\begin{aligned}
l_1^H w - l_2^H w &= l_1^H (w_r + jw_i) - l_2^H (w_r + jw_i) \\
&= (l_1^H - l_2^H) w_r + (jl_1^H - jl_2^H) w_i \\
&= \begin{bmatrix} l_1 - l_2 \\ -j(l_1 + l_2) \end{bmatrix}^H \begin{bmatrix} w_r \\ w_i \end{bmatrix} \\
&= D^H \bar{w} = [0, 0 \quad \ldots \quad 1]^T = g
\end{aligned}
\tag{19}
$$

The objective function in Eq. 13 can be written as

$$
\begin{aligned}
w^H R_x w &= (w_r + jw_i)^H R_x (w_r + jw_i) \\
&= \begin{bmatrix} w_r^H & w_i^H \end{bmatrix} \begin{bmatrix} R_x & jR_x \\ -jR_x & R_x \end{bmatrix} \begin{bmatrix} w_r \\ w_i \end{bmatrix} \\
&= \bar{w}^H \bar{R}_x \bar{w}
\end{aligned}
\tag{20}
$$

From the above derivation, Eq. 13 can be rewritten as

$$
\begin{aligned}
\bar{w} &= argmin \bar{w} \bar{R}_x \bar{w} \\
s.t. D^H \bar{w} &= g
\end{aligned}
\tag{21}
$$

It can be solved

$$\begin{bmatrix} w_r \\ w_i \end{bmatrix} = \bar{w} = \bar{R}_x^{-1} D \left(D^H \bar{R}_x^{-1} D \right)^{-1} g \tag{22}$$

$$\bar{w} = w_r + jw_i \tag{23}$$

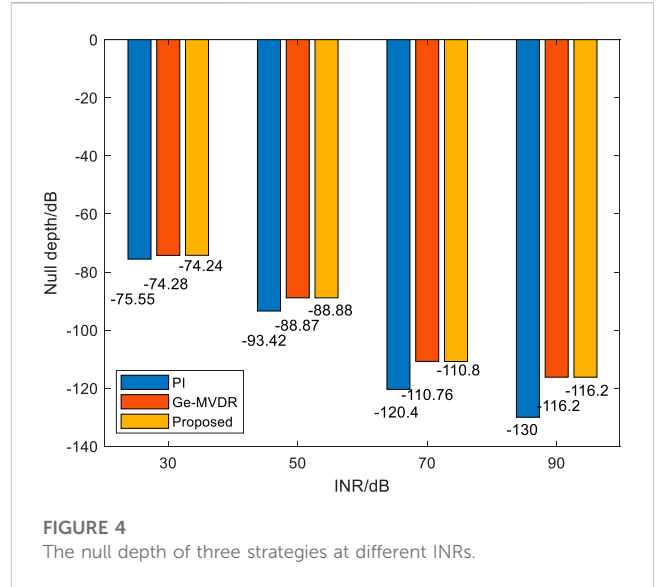The $H(f, \theta)$ of the proposed strategy can be described as

FIGURE 4
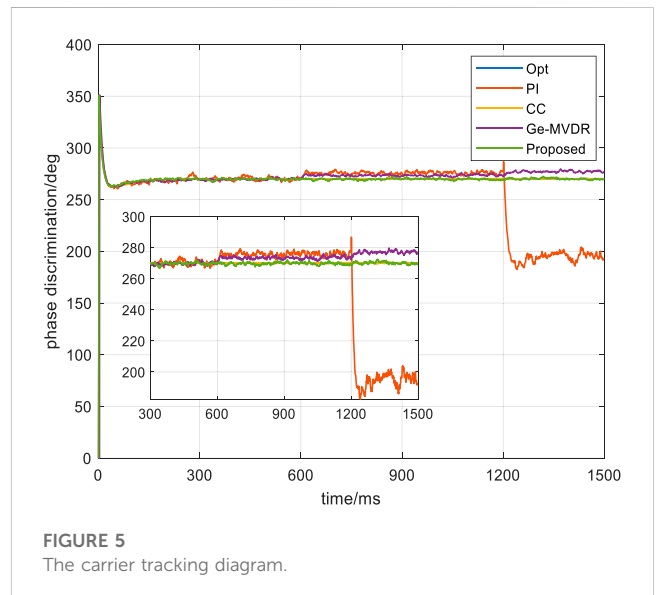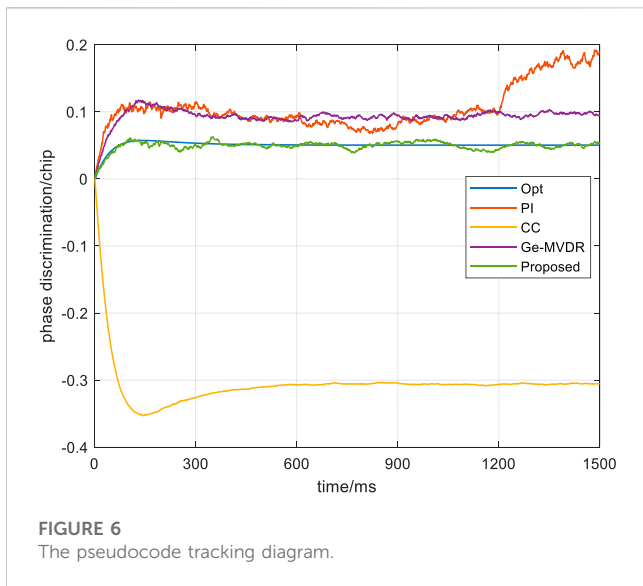The null depth of three strategies at different INRs.

FIGURE 5
The carrier tracking diagram.

$$H(f, \theta) = |H(f, \theta, \varphi)| exp \left[j2\pi f_0 \frac{M+1}{2} T_s \right] \tag{24}$$

Eq 24 satisfies the linear phase condition and has $(M+1)T_s/2$ phase shift. The cross-coherent is indicated as

$$
\begin{aligned}
R_2(\tau, \theta) &= cA_0 \int_{-\infty}^{\infty} \Phi(f) |H(f, \theta)| e^{j(\psi_0)} e^{j2\pi f (\tau - \tau_0 - (M+1)T_s/2)} df \\
&= \sum_{m=1}^{M} h(m) r(\tau - (m-1)T_s)
\end{aligned}
\tag{25}
$$

where $r(\tau)$ is the standard cross-coherent function between the navigation signal and its local copy. Eq 25 shows that the cross-coherent peak appears at the delayed position of the center-tap. The phase group delay of the cross-coherent is related to the number of delay taps, the sampling frequency and the delay direction. Increasing the sampling frequency or reducing the delay tap can reduce the group delay. However, reducing delay taps will lose the

FIGURE 6
The pseudocode tracking diagram.

$$R_2(\tau, \theta) = cA_0 \int_{-\infty}^{\infty} \Phi(f)|H(f, \theta)|e^{j(\psi_0)}e^{j2\pi f(\tau - \tau_0)}df \qquad (26)$$

It can be clearly displayed from Eq. 10 that the position of the cross-coherent peak is $\tau = \tau_0$ in the cross-coherent integral, and the phase angle of the peak is ψ_0. Therefore, the phase bias of the carrier is zero. Moreover, compared with references [18–20], the pseudocode phase offset of the proposed strategy is 0, which requires no additional processing in the subsequent fog computing, thus ensuring the accuracy of the system data and maintaining the computational complexity.

5 Results and discussion

An distributed wireless IoT system with a 4-element linear array is considered, and the satellite software simulator is used to generate the complex Beidou B1 band signal received by the 4-element linear array. The sampling frequency and time are set to 20 MHz and 1.5s, respectively. Array elements are placed equidistant with half wavelength. The complex signal of baseband IF 5.68 MHz is filtered by STAP. The number of delay nodes is 15. To test the effectiveness of the proposed strategy, the wideband continuous wave (WCW) interference and the wideband Gaussian noise (WGN) interference are added at t = 0.6s and t = 1.2s, respectively. The setting of interference scenarios is shown in Table 2.

The simulation of anti-interference null is carried out to verify the anti-interference capability in the distributed wireless IoT system. Figure 4 shows the null depth of traditional PI, Ge-MVDR method [22] and the proposed anti-interference strategy at different INRs during 600–1200 ms. The Monte Carlo experiment

degree of freedom (DOF), and increasing the sampling frequency will increase the computational complexity. To remove the group pseudocode offset so that the anti-interference processor can interface a generic receiver without modifying the receiver delay locked loop (DLL), the paper modified the STAP structure from the perspective of time delay direction as shown in Figure 3.

In Figure 3, the center tap is used as the input reference, and the output of the filter is obtained by accumulating the signals of each tap. Therefore, when the filter phase response is linear, the delay deviation of the pseudocode cross-coherent peak is the same as the time delay of the center tap, i.e., its delay is 0. The cross-coherent function is
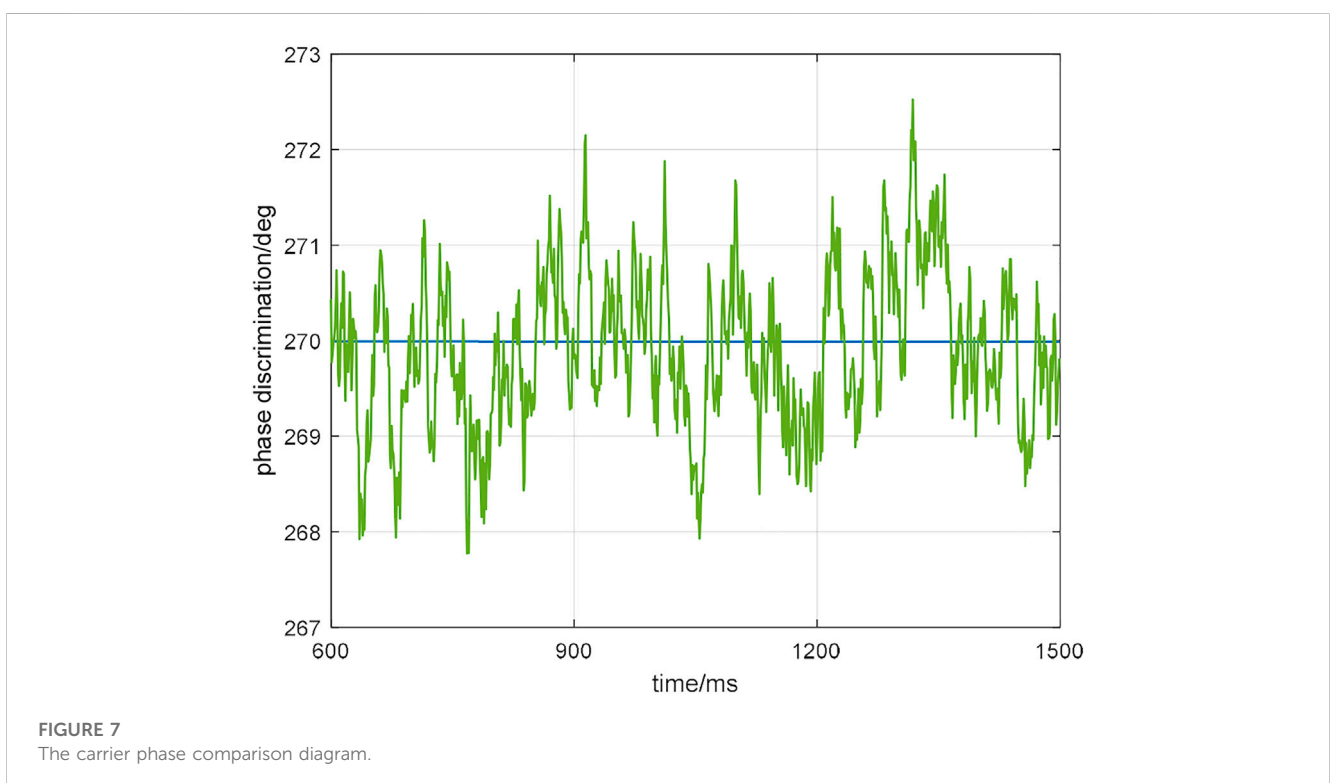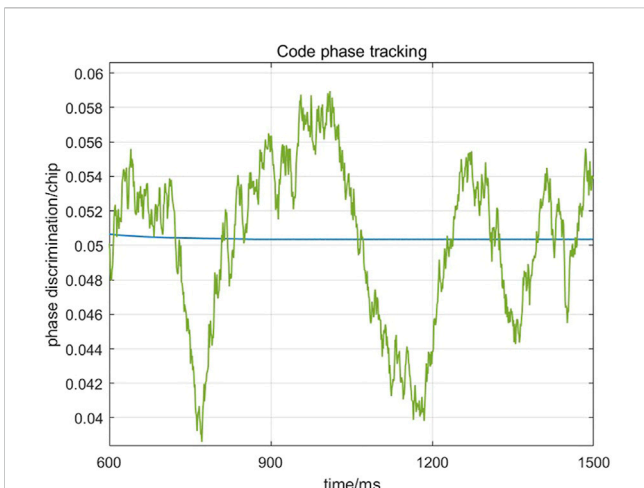

FIGURE 7
The carrier phase comparison diagram.

FIGURE 8
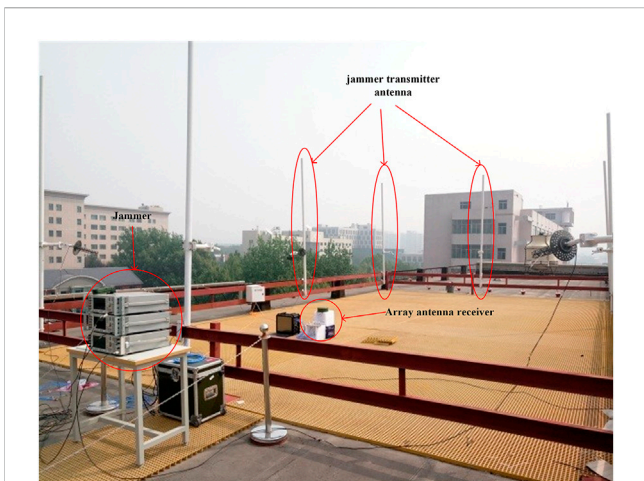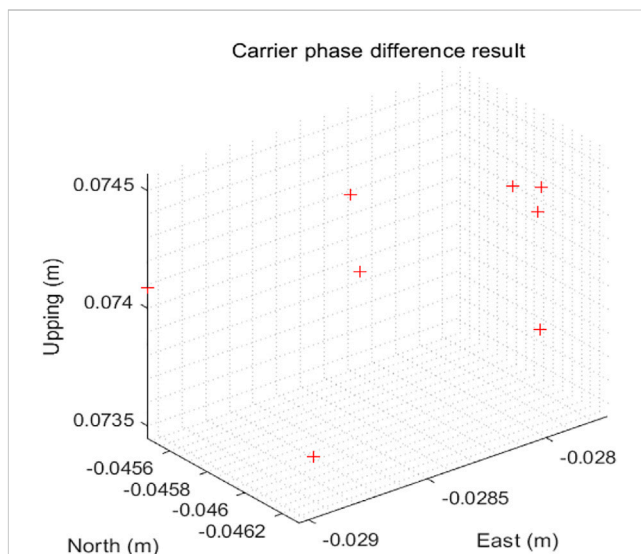The pseudocode phase comparison diagram.
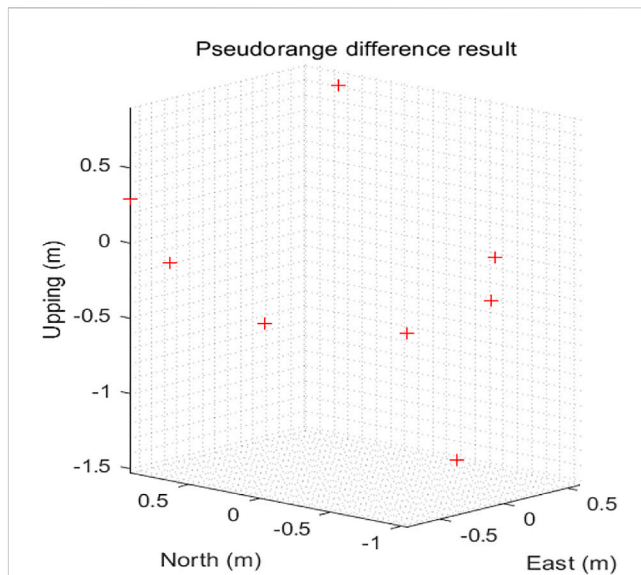
FIGURE 10
Pseudo-range differential positioning result diagram.

FIGURE 9
Experimental scene diagram.

FIGURE 11
Plot of carrier phase differential positioning results.

was performed 500 times. The anti-interference nulling of the proposed strategy is comparable to that of the Ge-MVDR method and slightly lower than that of the PI method, but it can still meet the required interference suppression.

Then, the baseband synchronization is performed by using an open-access software receiver [30]. To highlight the effectiveness of the algorithm, the PI method, the Ge-MVDR method and conjugate constraint (CC) method [19] are compared. Obviously, the tracking of the PI strategy and the Ge-MVDR strategy have errors as the scene changes in Figures 5, 6. At 600 ms and 1,200 ms, the carrier phase bias of the PI method is about 8° and 80°, and the carrier phase bias of the Ge-MVDR method is about 5° and 9°. In addition, after 600 ms, the pseudocode phase offset of the PI and Ge-MVDR is about 0.087 chips and 0.098 chips, and after 1,200 ms, the pseudocode phase offset of the PI and Ge-MVDR is about 0.17 chips and 0.1 chips. On the contrary, the CC method and the proposed strategy have no error, but the code

phase of the CC method still has a constant delay bias $(M + 1)T_s/2$, that is, there are 0.35 chip errors using the simulation parameters in this section. The proposed strategy is distortion-free.

For the residual error after applying the proposed strategy in the distributed wireless IoT system, the carrier phase and pseudocode phase are compared with the optimal value. Optimal values are generated in the environment without interference and noise. Figure 7 is a carrier phase comparison diagram. The carrier phase fluctuation range of the proposed strategy is ± 2.5°. The error of the carrier phase is within 0.14 cm. Figure 8 is a pseudocode phase comparison diagram. The fluctuation range of the pseudocode phase error is ±0.012 chips, that is, the error is within 3.517 m. These

FIGURE 12
The acquired satellite constellation map.
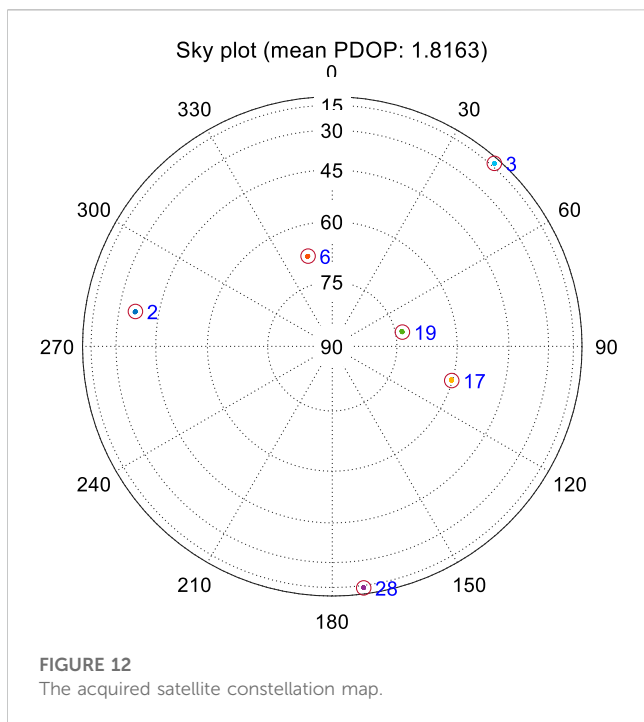
residuals are affected by noise, and can be further eliminated by smoothing the multiple positioning results.

To verify the high-precision positioning of the distributed wireless IoT system based on fog computing, the actual satellite signal and three interferences were received, as shown in Figure 9. HG-SOFTGPS02 GNSS intermediate frequency signal collector is utilized. The sampling frequency is 16.369MHz, and the IF is 4.1304 MHz. It is assumed that the reference station and the mobile station have achieved precise positioning in an interference-free environment, i.e., the positioning result is the true position. The calculation formula of the pseudo-range is

$$\rho = r + c \cdot (t_{sa} + t_u) + \varepsilon \qquad (27)$$

where r is the actual star-ground geometric distance, t_{sa} is the satellite clock difference, t_u is the receiver clock difference, and ε is the noise. c is the speed of light. The pseudo-range measured by the software receiver is

$$\rho = c \cdot \left(t_{travel} + t_{chip}\right) \qquad (28)$$

where t_{travel} is the signal propagation time and t_{chip} is the time corresponding to the code phase. When there is interference, the pseudo-range after STAP processing is written as

$$\rho_{stap} = c \cdot \left(t_{travel} + t_{chip} + t_{\Delta chip}\right) = r + c \cdot \left(t_s + t_u + t_{\Delta chip}\right) + \varepsilon \quad (29)$$

where $t_{\Delta chip}$ is the time corresponding to the code offset error.

For pseudo-range differential positioning, the accurate measurement information of the reference station is used to broadcast the correction parameters to the mobile station, which can eliminate the satellite clock error, receiver clock error and noise components of the mobile station to achieve accurate measurement. To verify the effect of pseudocode phase deviation on high-precision positioning, it is sufficient to add the distance corresponding to the

pseudocode phase deviation to the accurate measurement information. Figure 10 shows the results of pseudo-range differential positioning. The positioning error of east, north and altitude are less than 1 m.

Similarly, for the effect of carrier phase deviation on high-precision positioning, it is only necessary to add the distance corresponding to the carrier phase measurement deviation to the accurate measurement information. Figure 11 shows a plot of the carrier phase differential positioning results. The positioning error of east, north and altitude are less than 10 cm. Figure 12 is the constellation diagram of the acquired satellite signals.

6 Conclusion

To ensure that the navigation data is accurate and not interfered during broadcast/reception of each fog computing node in the distributed wireless IoT system based on high-precision positioning, an unbiased STAP anti-interference strategy is proposed in this paper. By reconstructing the equivalent filter structure and constraining the filter coefficients, this proposed strategy eliminates pseudocode shift and carrier phase bias due to the non-linear response of STAP systems, which can effectively improve the anti-interference performance and high-precision positioning capabilities of wireless IoT such as the Internet of Vehicles, intelligent logistics and disaster warning. The experiment results state that the error result of pseudo-range differential positioning is less than 1m, and the error result of carrier phase differential positioning is less than 10 cm.

Data availability statement

The datasets presented in this article are not readily available because There is a foundation for long-term project cooperation between us. Requests to access the datasets should be directed to FH, hf791350398@163.com.

Author contributions

Conceptualization, FH and WW; Methodology, FH, XL, and WW; Software, FH Validation, FH, WW, and JZ, Formal analysis, FH and XL; Writing—original draft preparation, FH Writing—review and editing, FH, WW, XL, and JZ

Funding

Conflict of interest

The authors declare that the research was conducted in the absence of any commercial or financial relationships that could be construed as a potential conflict of interest.

Publisher's note

All claims expressed in this article are solely those of the authors and do not necessarily represent those of their affiliated organizations, or those of the publisher, the editors and the reviewers. Any product that may be evaluated in this article, or claim that may be made by its manufacturer, is not guaranteed or endorsed by the publisher.

References

1. Wang L, Li L, Qiu R. Edge computing-based differential positioning method for BeiDou navigation satellite system. *KSII Trans Internet Inf Syst* (2019) 13:69–85. doi:10.3837/tiis.2019.01.005

2. Zhang PY, Wang YQ, Kumar N, Jiang CX, Shi GW. A security and privacy-preserving approach based on data disturbance for collaborative edge computing in social IoT systems. *IEEE Trans Comput Soc Syst* (2022) 9:97–108. doi:10.1109/TCSS.2021.3092746

3. Zhang PY, Jiang CX, Pang X, Qian Y. STEC-IoT: A security tactic by virtualizing edge computing on IoT. *IEEE Internet Things J* (2021) 8:2459–67. doi:10.1109/jiot.2020.3017742

4. Ni SJ, Ren BB, Chen FQ, Lu ZK, Wang J, Ma PC, et al. GNSS spoofing suppression based on multi-satellite and multi-channel array processing. *Front Phys* (2022) 10:10. doi:10.3389/fphy.2022.905918

5. Ren BB, Chen FQ, Ni SJ, Han C, Lu Z, Han S. Performance analysis of repeater spoofing suppression based on GNSS multi-beam receiver. *Front Phys* (2022) 10:10. doi:10.3389/fphy.2022.970132

6. Yang X, Li S, Sun Y, Long T, Sarkar TK. Robust wideband adaptive beamforming with null broadening and constant beamwidth. *IEEE Trans Antennas Propagation* (2019) 67:5380–9. doi:10.1109/TAP.2019.2916607

7. Wang H, Yao Z, Fan Z, Yang J, Liu G. A robust STAP beamforming algorithm for GNSS receivers in high dynamic environment. *Signal Process.* (2020) 172:107532–10. doi:10.1016/j.sigpro.2020.107532

8. Church C, Gupta I, O'Brien A. Adaptive antenna induced biases in GNSS receivers. In: Proceedings of the 63rd Annual Meeting of The Institute of Navigation; -25 April 2007; Cambridge, Massachusetts (2007). p. 204–12.

9. Chuang YC, Gupta IJ. Antenna induced biases in GNSS receiver measurements. In: Proceedings of the 2013 International Technical Meeting of The Institute of Navigation; January 29 - 27, 2013; San Diego, California (2013). p. 164–71.

10. Lee K, So H, Song K. Performance analysis of pseudorange error in STAP beamforming algorithm for array antenna. *J Positioning, Navigation, Timing* (2014) 3:37–44. doi:10.11003/JPNT.2014.3.2.037

11. Daneshmand S, Jahromi AJ, Broumandan A, Lachapelle G. GNSS space-time interference mitigation: Advantages and challenges. In: Proceedings of the International Symposium on GNSS (IS-GNSS '15); July 7 and 8, 2015; Darmstadt, Germany (2015). p. 11.

12. Daneshmand S, Jahromi AJ, Broumandan A, Lachapelle G. GNSS space-time interference mitigation and attitude determination in the presence of interference signals. *Sensors* (2015) 15:12180–204. doi:10.3390/s150612180

13. Vagle N, Broumandan A, Jafarnia A. Characterization of GNSS measurement distortions due to antenna array processing in the presence of interference signals. In: 2014 Ubiquitous Positioning Indoor Navigation and Location Based Service (UPINLBS); November 20-21,2014; TX, USA (2014). p. 71–80.

14. Fante RL, Vaccaro JJ. Wideband cancellation of interference in a GPS receive array. *IEEE Trans Aerospace Electron Syst* (2000) 36:549–64. doi:10.1109/7.845241

15. Wu R, Xu R, Lu D. STAP compensation technique based on homomorphic filtering in GPS. In: 2010 IEEE International Symposium on Phased Array Systems and Technology; October 12–15, 2010; Boston (2010). p. 841–5.

16. O'Brien AJ, Gupta IJ. An optimal adaptive filtering algorithm with zero antenna-induced bias for GNSS antenna arrays. *Navigation* (2010) 57(2):87–100. doi:10.1002/j.2161-4296.2010.tb01769.x

17. O'Brien AJ, Gupta IJ. Mitigation of adaptive antenna induced bias errors in GNSS receivers. *IEEE Trans Aerospace Electron Syst* (2011) 47(1):524–38. doi:10.1109/TAES.2011.5705689

18. Wang Y, Liu W, Huang L, Xiao Z, Wang F. Distortionless pseudo-code tracking space–time adaptive processor based on the PI criterion for GNSS receiver. *IET Radar, Sonar and Navigation* (2020) 14:1984–90. doi:10.1049/iet-rsn.2020.0189

19. Chen F, Nie J, Li B, Wang F. Distortionless space-time adaptive processor for global navigation satellite system receiver. *IEEE Elect Lett* (2015) 51:2138–9. doi:10.1049/el.2015.2832

20. Xu H, Cui X, Lu M. Adaptive blind nulling without measurement biases in GNSS receivers. In: 2017 IEEE 17th International Conference on Communication Technology (ICCT); 27-30 October 2017; Chengdu, China (2017). p. 1074–8.

21. Dai X, Nie J, Chen F, Ou G. Distortionless space-time adaptive processor based on MVDR beamformer for GNSS receiver. *IET Radar Sonar Navigat* (2017) 11:1488–94. doi:10.1049/iet-rsn.2017.0168

22. Marathe T, Daneshmand S, Lachapelle G. Assessment of measurement distortions in GNSS antenna array space-time processing. *Int J Antennas Propagation* (2016) 2016:1–17. doi:10.1155/2016/2154763

23. Liu F, Zhang M, Gao F. MWF-NW algorithm for space-time antijamming. *Prog Electromagnetics Res M* (2019) 78:165–74. doi:10.2528/PIERM18120504

24. Wang H, Yao Z, Fan Z, Yang J, Liu G. A robust STAP beamforming algorithm for GNSS receivers in high dynamic environment. *Signal Processing* (2020) 6:107532–. doi:10.1016/j.sigpro.2020.107532

25. Wang X, Xu D, Wang W, Han Z. Robust beamformer based on magnitude response constraint and steering vector correction. *Elect Lett* (2015) 51:1302–4. doi:10.1049/el.2015.0968

26. Li Q, Wang W, Xu D, Wang X. A robust anti-jamming navigation receiver with antenna array and GPS/SINS. *IEEE Commun Lett* (2014) 18:467–70. doi:10.1109/LCOMM.2014.012314.132451

27. Khan M, Agha S. Least squares linear phase FIR filter design and its VLSI implementation. *Analog Integrated Circuits Signal Process.* (2020) 105:99–109. doi:10.1007/s10470-020-01688-9

28. Wang PH, Yu BY, Chen PN. Type II, III, and IV linear-phase FIR structures based on cardinal filters. *IEEE Trans Circuits Syst Express Briefs* (2019) 66:1920–4. doi:10.1109/TCSII.2019.2892484

29. Richard G. *Understanding digital signal processing*. Upper Saddle River, New Jersey, USA: Prentice Hall PTR (2010).

30. Borre K, Akos D. A software-defined GPS and galileo receiver: Single-frequency approach. In: Proceedings of the 18th International Technical Meeting of the Satellite Division of The Institute of Navigation; Sept. 13-16, 2005; Long Beach (2005). p. 1632–7. ION GNSS 2005).